HHS Public Access

Author manuscript

Eur J Neurosci. Author manuscript; available in PMC 2022 November 09.

Published in final edited form as:

Eur J Neurosci. 2021 November ; 54(10): 7654–7667. doi:10.1111/ejn.15485.

Surface values, volumetric measurements, and radiomics of structural MRI for the diagnosis and subtyping of attention-deficit/hyperactivity disorder

Liting Shi[1,2], **Xuechun Liu**[4], **Keqing Wu**[2,5], **Kui Sun**[4], **Chunsen Lin**[6], **Zhengmei Li**[4], **Shuying Zhao**[4,7], **Xiuqin Fan**[3]

[1.]School of Biomedical Engineering (Suzhou), Division of Life Sciences and Medicine, University of Science and Technology of China, Hefei, Anhui, China

[2.]Department of Medical Imaging, Suzhou Institute of Biomedical Engineering and Technology, Chinese Academy of Science, Suzhou, Jiangsu, China

[3.]Laboratory of Nutrition and Development, Key Laboratory of Major Diseases in Children, Ministry of Education, Beijing Pediatric Research Institute, Beijing Children's Hospital, Capital Medical University, National Center for Children's Health, Beijing, China

[4.]Medical Engineering and Technology Research Center; Department of Radiology, Shandong First Medical University & Shandong Academy of Medical Sciences, Taian, China

[5.]School of Computer Engineering and Science, Shanghai University, Shanghai, China

[6.]Department of Radiology, Taian Disabled soldiers' Hospital of Shandong Province, Taian, China

[7.]The National Clinical Research Center for Mental Disorders & Beijing Key Laboratory of Mental Disorders, Beijing Anding Hospital, Capital Medical University, Beijing, China

Abstract

Attention-deficit/hyperactivity disorder (ADHD) is diagnosed subjectively based on an individual's behaviour and performance. The clinical community has no objective biomarker to inform the diagnosis and subtyping of ADHD. This study aimed to explore the potential diagnostic biomarkers of ADHD among surface values, volumetric metrics, and radiomic features that were extracted from structural MRI images. Public data of New York University and Peking University were downloaded from the ADHD-200 consortium. MRI T1-weighted images were pre-processed using CAT12. We calculated surface values based on the Desikan-Killiany atlas. The volumetric metrics (mean grey matter volume and mean white matter volume) and radiomic

Address for correspondence: Xiuqin Fan, Beijing Children's Hospital, Capital Medical University, No. 56 Nan-li-shi Road, Beijing 100045, China. Tel: 86-010-59616895, qincaifan@126.com.

Author contributions statement

L.S. and X.F. conceived and designed the experiments. X.L. calculated surface values and volumetric measurements. L.S. extracted radiomic features. L.S., K.W., and K.S. analysed the data. X.F., X.L., and L.S. wrote the draft. All authors provided critical feedback, helped shape the analysis and manuscript, and approved the final version of the manuscript.

Conflicts of Interest

No.

Ethical statement

The authors are accountable for all aspects of the work in ensuring that questions related to the accuracy or integrity of any part of the work are appropriately investigated and resolved.

features within each AAL brain area were calculated using DPABI and IBEX, respectively. The differences among three groups of participants were tested using ANOVA or Kruskal-Wallis test depending on the normality of the data. We selected discriminative features and classified typically developing controls (TDCs) and ADHD patients as well as two ADHD subtypes using least absolute shrinkage and selection operator and support vector machine algorithms. Our results showed that the radiomics-based model outperformed the others in discriminating ADHD from TDC as well as classifying ADHD subtypes (area under curve [AUC]: 0.78 and 0.94 in training test; 0.79 and 0.85 in testing set). Combining grey matter volumes, surface values, and clinical factors with radiomic features can improve the performance for classifying ADHD patients and TDCs with training and testing AUCs of 0.82 and 0.83, respectively. This study demonstrates that MRI T1-weighted features, especially radiomic features, are potential diagnostic biomarkers of ADHD.

Graphical Abstract

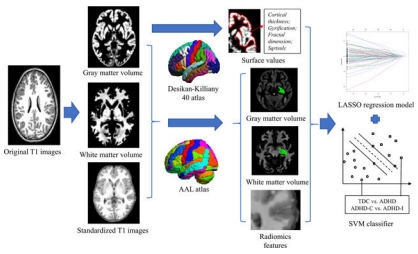

Structural MRI T1-weighted image-extracted features can distinguish patients with attention-deficit/hyperactivity disorder (ADHD) from typically developing controls as well as between the inattentive and combined subtypes. Radiomic features showed better performance than surface values, grey matter volume, white matter volume, and clinical factors. Combining other categories of features with radiomic features to build a hybrid model can improve the performance for the diagnosis of ADHD.

Keywords

attention-deficit/hyperactivity disorder; MRI T1-weighted images; radiomics; surface values; volumetric measurements

Introduction

Attention-deficit/hyperactivity disorder (ADHD) is a disabling neurodevelopmental disease that can cause inattention and aberrant hyperactive/impulsive behaviours in children and adults (Polanczyk & Rohde, 2007). ADHD can be diagnosed as three types: inattentive (ADHD-I), hyperactive/impulsive (ADHD-H/I), and combined (ADHD-C) (NIMH). Symptoms of ADHD-I include being disorganized, a lack of persistence, and difficulties in sustaining focus/attention, while ADHD-H/I exhibits as fidgeting and squirming in seats, moving about, or talking constantly even in inappropriate situations, and making hasty actions (NIMH). ADHD affects 5–10% of school-age children, but its symptoms can be misinterpreted as emotional or disciplinary problems, thus bringing

serious lifelong impairments such as failing relationships and impaired academic and work performance. Clinical and basic research on ADHD has been ongoing for more than a century, focusing on the biological causes of hyperactivity, impulsivity, and attention deficit (Berger & Posner, 2000; Overmeyer et al., 2001; Visser et al., 2014). However, ADHD diagnosis was still assessed subjectively based on individual behaviour and performance. There remains no objective biomarker to inform the diagnosis of ADHD in the clinical community.

Since the introduction of magnetic resonance imaging (MRI) that allows in vivo measurement of brain structures (R. A. Yotter, Nenadic, Ziegler, Thompson, & Gaser, 2011), using magnetic resonance brain imaging to diagnose disease makes the results more objective. Some structural MRI-based studies have shown developmental changes in the volume of the cortical and subcortical areas in those with ADHD (C. U. Greven et al., 2015; Hoogman et al., 2017; Tomohiro, Joaquim, Katya, & David, 2011; Valera, Faraone, Murray, & Seidman, 2007; Vilgis, Sun, Chen, Silk, & Vance, 2016). A simultaneous delay in the development of cortical thickness and surface area suggests that there may be a global perturbation of cortical maturation in ADHD, as reported by the National Institute of Mental Health (NIMH) (P Shaw et al., 2007; Philip Shaw et al., 2012). Some studies used region-of-interest (ROI)-based measurements or voxel-based methods (VBM) to identify the specific brain structures and potential markers (such as grey matter (GM) volume, surface area, and thickness) that are capable of diagnosing ADHD using statistical analysis (Brinson, 2014; Chi-Hua et al., 2013; Frodl & Skokauskas, 2012; Lu et al., 2019; Zhao et al., 2020). However, the findings in these studies were inconsistent. Alterations in GM volume, surface area, and inward deformation in different regions (such as the left frontal eye field, the left middle cingulum, and left cuneus) were reported in patients with ADHD compared to typically developing controls (TDCs) by some groups (Lu et al., 2019; Tang et al., 2019; Zhao et al., 2020), while no difference was found in the local distribution of GM by other studies (Ulke et al., 2019).

Several new methods have been proposed to find potentially subtle structural differences on structural MRI images. Radiomics is a new technique that has emerged from the medical field of oncology and has recently been used to analyse structural and functional MRI (fMRI) images in the field of neurology (Aerts et al., 2014; Yupeng Li et al., 2019; Y. Li, Jiang, Shen, Wu, & Zuo, 2018; Port, 2018; Sun et al., 2018). Radiomic features are statistical descriptors that can quantify the spatial relationship in the grey level of voxels in images. In a previous study, a single-institutional model combining GM- and white matter (WM)-based radiomic features could diagnose ADHD and classify the subtypes, but the classification accuracy was limited (73.7% and 80.1%) (Sun et al., 2018). It is still unknown whether radiomic features extracted directly from brain structural MRI images that do not separate GM and WM can provide more diagnostic information for ADHD.

Surface-based morphometry allows the measurement of four surface values that describe cortical folding patterns in detail (Gutman, Wang, Morra, Toga, & Thompson, 2009), including cortical thickness (Draper, Jackson, Morgan, & Jackson, 2016), gyrification (Luders et al., 2006), fractal dimension (Corbit & Garbary, 1995), and sqrtsulc (Gaser & Dahnke, 2016). Cortical thickness is the average local orthogonal distance between the

voxels of the grey/white boundary and the grey/cerebrospinal fluid boundary (Dahnke, Yotter, & Gaser, 2013). Gyrification measures the surface complexity based on absolute mean curvature (Luders et al., 2006; R. A Yotter, Nenadic, Ziegler, Thompson, & Gaser, 2011b). The fractal dimension represents cortical complexity (R. A Yotter et al., 2011b). The sqrtsulc is defined as the square root-transformed sulcus depth based on the Euclidean distance between the central surface and its convex hull (Gaser & Dahnke, 2016). A previous study reported that the top discriminative features for ADHD were in cortical areas (Sun et al., 2018), and the surface values were associated with multiple brain diseases (Al-Radaideh, Athamneh, Alabadi, & Hbahbih, 2019; Madeira et al., 2020; Wolf et al., 2020; Zheng et al., 2019). The discriminative ability of the four surface values for the diagnosis of ADHD has not been investigated until now.

The purpose of this study was to identify diagnostic biomarkers for ADHD among some novel quantitative features of structural MRI images, i.e., surface values, volumetric measurements, and radiomic features, using multi-institutional data from the ADHD-200 consortium. Statistical analysis was used to explore specific brain areas/cortical structures and corresponding features showing significant differences among TDCs, ADHD-C patients, and ADHD-I patients. Furthermore, we established machine learning models using each category of features within multiple brain areas/cortical structures and their combination to evaluate their diagnostic performance for individual participants.

Materials and Methods

Datasets

Public structural MRI data of New York University (NYU) Child Study Centre and Peking University (PU) were downloaded from the ADHD-200 Consortium (http://fcon_1000.projects.nitrc.org/indi/adhd200/index.html) (HD-200, 2012). ADHD diagnoses were based on the Schedule of Affective Disorders and Schizophrenia for Children-Present and Lifetime Version (KSADS-PL) administered to children and parents and the Conners' Parent Rating Scale-Revised, Long version (CPRS-LV). Patients were included if they (1) had available phenotypic data and MRI images and (2) passed the quality control of anatomical images. Patient exclusions were (1) left-handedness and (2) abnormal clinical phenotypes (such as ADHD index, inattentive score, and hyper/impulsive score) (equal to −999). ADHD-H/I patients were also excluded due to the small sample size (NYU: 2; PU: 1). Finally, 155/166 participants aged 7–18/8–16 years at NYU/PU were selected for analysis. Table 1 shows all participants' demographic information. All images were acquired using a Siemens Allegra 3.0 T scanner at NYU and a Siemens TrioTim 3.0T scanner at PU for brain imaging, with a high-resolution T1-weighted MPRAGE 3D volume. The detailed parameters were as follows: slice thickness = 1.33 mm, slices per slab =128, repetition time (TR) = 2530 ms, echo time (TE) = 3.25 ms (NYU) and 3.39 ms (PU), field of view (FOV) read = 256 mm, and voxel size: 1.3×1.0×1.3 mm. The total acquisition time (scan time) was 8:07 minutes.

Image pre-processing

Figure 1 shows the workflow of this study. First, all original NIfTI data were reoriented and cropped using DCM2NII (https://people.cas.sc.edu/rorden/mricron/dcm2nii.html). The image quality was checked based on the following criteria: a) images had no motion artefact, b) the scanning range completely enveloped the brain tissue, and c) the head was not over-rotated. Images that did not pass the quality check or those with serious head movement were removed from the analysis. Next, we performed image pre-processing using the MATLAB (R2013b) toolbox cat12 (Computational Anatomy Toolbox 12, vCAT12.1, http://www.neuro.uni-jena.de/cat/) (Gaser & Dahnke, 2016), which is an extension of SPM12 (Statistical Parametric Mapping 12, https://www.fil.ion.ucl.ac.uk/spm/software/spm12/). The pre-processing included image reconstruction, correction, registration, and segmentation. The cat12 toolbox parameters were as follows: the spatial registration template was Dartel; the voxel size for normalized images was 1.5 mm × 1.5 mm × 1.5 mm; the hemispheres were not merged, thus resampled data were saved separately for each hemisphere; the resample size was 164k mesh (FreeSurfer); and the smoothing filter size in FWHM was 15 mm. Standardized GM volume images, standardized white matter (WM) volume images, and standardized T1 images with scalp stripping were exported after the pre-processing was finished. We checked the quality of the exported images, and participants with low-quality images were excluded from the analysis. Then, resampling and smoothing were applied to the images to make the data obey a normal distribution.

Feature extraction

As shown in Figure 1, ROI-based surface values, volumetric measurements, and radiomic features were extracted from the pre-processed images. First, the surface values, including cortical thickness, gyrification, fractal dimension, and sqrtsulc, were extracted based on the Desikan-Killiany 40 (DK) atlas (72 cortical structures) after the pre-processed images were aligned to the MNI152 template space using cat12 (Gaser & Dahnke, 2016; R. A Yotter et al., 2011b). Second, we extracted the volumetric measurements (mean GM volume and mean WM volume) inside the brain areas defined by the automated anatomical labelling (AAL) atlas (116 brain areas) after importing the cat12 exported standardized volume images to Dpabi (V4.2_190919) (Yan, Wang, Zuo, & Zang, 2016). Finally, 209 radiomic features within each AAL area on standardized T1 images and a total of 209*116 radiomic features were extracted using open source software, IBEX source (V1.0β) (Aerts et al., 2014; Zhang et al., 2015). The radiomic features included first-order statistical features derived directly from the image intensity and intensity histogram (e.g., skewness, kurtosis, and variance) and high-order texture features calculated based on the grey-level cooccurrence matrix (GLCM), grey-level run length matrix (GLRLM), and neighbourhood intensity difference matrix (NIDM). The texture features were averaged over all 3D directions as the final feature values to approach a rotationally invariant system.

Statistical analysis

We calculated the differences in surface values, volumetric measurements, and radiomic features among the three groups of participants. The Lilliefors test and Bartlett test were used to determine whether the data of one feature obeyed a normal distribution with equal

variances. We used one-way analysis of variance (ANOVA) for the normally distributed data and the Kruskal-Wallis test for the nonnormally distributed data to calculate the differences in all data among the three groups. The Bonferroni method was applied to all results to correct multiple testing problems, where corrected $P < 0.05$ was considered as statistically significant. A multiple comparison test was used to further investigate the differences between each pair of the three groups in those features with corrected $P < 0.05$.

Furthermore, the association of brain and age was investigated for TDCs and ADHD patients separately using Spearman's rank correlation coefficient, and the difference in the association between the two groups was evaluated using a two-sample two-sided t test. Bonferroni correction was applied to the results of the t test, where corrected $P < 0.05$ was statistically significant.

Feature selection and classification

All data were normalized to a range of 0 to 1 using min-max normalization. We classified the TDCs and patients with ADHD using all 321 participants' data, and classified ADHD-C patients and ADHD-I patients using 151 ADHD participants' data. For each classifier, all participants were randomly allocated into the training set and the testing set using a ratio of 3:1. We selected the most diagnostic features using the least absolute shrinkage and selection operator (LASSO) algorithm, which performs feature selection and regularization to improve the overall performance and interpretability of the model (Friedman, Hastie, & Tibshirani, 2010; Tibshirani, 2011). This algorithm has been widely used in recent MRI-based machine learning studies and has shown advantages over other feature selection algorithms (Lohmann et al., 2021; Park et al., 2020). During the training of a LASSO model, the area under the receiver operating characteristic curve (AUROC) between two classes was maximized by tuning parameter (λ) in a 10-fold cross validation using data in the training set. The minimum criterion or one standard error criterion was adopted depending on its performance in the training set. Most covariate coefficients simultaneously shrank to zero, and those features with nonzero coefficients were finally selected by LASSO. The selected features of participants in the training set were used to train an SVM model with a radial basis function (RBF) kernel and optimize the classification performance in the 10-fold cross validation. The SVM algorithm performs reasonably well with small sample-sized data and has shown excellent performance in brain image analysis (Nguyen, Blears, Ross, Lall, & Ortega-Barnett, 2018; Sordo & Zeng, 2005; Wu et al., 2019). The combination of LASSO and SVM can avoid possible overfitting during feature selection and model training and has recently been used in neuroimage-based radiomics studies (Wang et al., 2020). For each classification task, we established five single LASSO-SVM models using clinical factors (Table 1), grey matter volumes, white matter volumes, surface values, and radiomic features and combined all of them to build a hybrid LASSO-SVM model. The final trained model was used to predict the class of participants in the testing set. A receiver operating characteristic (ROC) curve illustrated the classification ability of the trained model, while the area under the curve (AUC) was simultaneously calculated. Feature selection and classification were carried out using R version 4.0.4.

Results

Statistical analysis

After Bonferroni correction, 142 radiomic features of 18 brain areas (AAL numbers: 12, 17, 18, 29, 30, 32, 39, 63, 79–82, 85, 87, 91, 95, 105, and 106) and the cortical thickness of 'linsula' were statistically significant among the three groups of participants (corrected ANOVA P = 1.91×10^{-4}-0.05). In the multiple comparison test, all these features showed significant differences between TDCs and ADHD-C patients (P = 2.09×10^{-9}-5.73×10^{-5}); 20 radiomic features of 4 brain areas (AAL numbers: 63, 79, 80, and 81) (AAL numbers:) had significant differences between TDCs and ADHD-I patients (P = 2.29×10^{-5}-0.05); ADHD-C patients significantly differed from ADHD-I patients in 109 radiomic features of 14 brain areas (AAL numbers: 12, 17, 18, 29, 30, 32, 39, 63, 80, 81, 87, 91, 105, 106) (P = 1.53×10^{-4}-0.05). Only two radiomic features ('30 percentile' and '0.25 quantile') of 'Heschl_R' and one radiomic feature ('10 percentile') of 'Temporal_Sup_L' showed significant differences in all pairwise comparisons of the three groups (P = 3.31×10^{-9}-0.05). Figure 2 shows boxplots and data distribution of cortical thickness of 'linsula' and '30 percentile' of 'Heschl_R' among three groups of participants in two medical centres (corrected ANOVA P = 0.05 and 2.41×10^{-3}). All results of the statistical analysis are shown in supplementary Table S1.

For the association of brain and age, ADHD patients differed from TDCs in grey matter volume, white matter volume, sqrtsulc, cortical thickness, and 30 radiomic features (28 first-order features and 2 texture features) (corrected P = $4.36*10^{-13}$, $9.12*10^{-23}$, 0.01, $4.49*10^{-8}$, and $5.02*10^{-12}$-0.04, respectively) (supplementary Table S2).

The classification of TDCs and patients with ADHD

Figure 3 shows the confusion matrices of all features in classifying TDCs and patients with ADHD in the testing set. The hybrid LASSO-SVM model integrating 10 radiomic features, 3 surface values, 1 grey matter volume, and 2 clinical factors outperformed any single model in both the training set (AUC [95% CI]: 0.82 [0.77–0.87]; sensitivity: 61.21%; specificity: 89.60%) and testing set (AUC [95% CI]: 0.83 [0.73–0.92]; sensitivity: 68.57%; specificity: 93.33%) (Figure 4). The SVM classification results and LASSO-selected features and their corresponding brain areas/cortical structures of all models are shown in Supplementary Tables S3 and S4, respectively.

For single models, the radiomics model achieved better performance than the other models in discriminating between TDCs and patients with ADHD (AUC [95% CI]: 0.78 [0.73–0.84] and 0.79 [0.69–0.90]; sensitivity: 83.62% and 82.85%; specificity: 56.00% and 71.11% in the training and testing sets, respectively). The discriminative radiomic features were seven first-order features of seven brain areas (AAL numbers: 20, 21, 30, 87, 88, 91, and 97) and two texture features of 'Cerebelum_9_R' (supplementary Table S4). The single models built using clinical factors, surface values, grey matter volumes, and white matter volumes also showed discriminative power between TDCs and ADHD patients (AUC: 0.71–0.80 and 0.63–0.74 in the training and testing sets, respectively) (supplementary Table S3 and Figure 4).

The classification of ADHD-C patients and ADHD-I patients

Figure 5 shows the confusion matrices of all features in classifying ADHD-C patients and ADHD-I patients in the testing set. The radiomic feature-based model performed the best in discriminating between the two subtypes of ADHD (AUC [95% CI]: 0.94 [0.91–0.99] and 0.85 [0.72–0.98]; sensitivity: 95.65% and 85.29%; specificity: 84.21% and 83.33% in the training and testing sets, respectively) (Figure 6 and supplementary Table S5). The discriminative radiomic features included 5 texture features of 4 brain areas (AAL numbers: 6, 10, 37, and 51) and 18 first-order features of 13 brain areas (AAL numbers: 14, 35, 41, 42, 44, 48, 49, 63, 69, 71, 95, 109, and 113) (supplementary Table S6). Combining other categories of features with radiomic features to build a hybrid model did not improve the discriminative power (AUC [95% CI]: 0.94 [0.90–0.98] and 0.83 [0.69–0.97]; sensitivity: 89.13% and 94.74%; specificity: 85.29% and 66.67% in the training and testing sets, respectively). Here, the sensitivity was defined as the accuracy in the ADHD-I group, while the specificity was defined as the accuracy in the ADHD-C group.

The other single models only showed limited discriminative power for classifying the two subtypes of ADHD (AUC: 0.69–0.75 and 0.60–0.66 in the training and testing sets, respectively) (supplementary Table S5 and Figure 6).

Discussion

This study explored diagnostic biomarkers for ADHD among ROI-based features calculated from structural MRI images, including DK atlas-based surface values and AAL-based mean GM volume, mean WM volume, and radiomic features. The major finding was that 142 radiomic features of 18 brain areas and cortical thickness of ‘linsula’ (a surface value) showed significant differences among the TDC, ADHD-C, and ADHD-I groups (corrected ANOVA $P = 1.91\times10^{-4}$-0.05). Among them, two radiomic features (‘30 percentile’ and ‘0.25 quantile’) of ‘Heschl_R’ and one radiomic feature (‘30 percentile’) of ‘Temporal_Sup_L’ had statistically significant differences in all pairwise comparisons of the three groups in the multiple comparison test ($P = 3.31\times10^{-9}$-0.05). Additionally, ADHD patients and TDCs had significant differences in the association of brain and age, which can be quantified by grey matter volume, white matter volume, sqrtsulc, cortical thickness, and 30 radiomic features. Furthermore, we established LASSO-SVM models using each category of features and their combination to classify ADHD and TDC as well as ADHD-C and ADHD-I. The radiomic feature-based LASSO-SVM model outperformed the other single models in diagnosing ADHD as well as separating ADHD-C patients from ADHD-I patients. The discriminative radiomics included first-order features and texture features of multiple brain areas. The other single models built using surface values, clinical factors, grey matter volumes, and white matter volumes also showed discrimination between TDC and ADHD. In addition, combining surface values, grey matter volume, and clinical factors with radiomic features to build a hybrid model can slightly improve classification performance for the diagnosis of ADHD but not for the discrimination between the two ADHD subtypes. Therefore, structural MRI features of multiple brain areas are potential biomarkers for the clinical diagnosis and subtyping of ADHD.

The ADHD-200 Global Competition was organized to find the best tools to diagnose patients with ADHD based on functional and structural MRI images (Brown et al., 2012; Guo, An, Kuang, Zhao, & He, 2014; Sato, Hoexter, Fujita, & Rohde, 2012). The winner of the competition was a team from Johns Hopkins University. They correctly identified 94% of TDCs but only 21% of ADHD cases, resulting in an accuracy of 61% (HD-200, 2012). Some fMRI-based studies reported that the accuracies of distinguishing ADHD from TDC or other brain diseases were 85%−86.5% (Rish et al., 2009; Shen, Wang, Liu, & Hu, 2010; Zhu et al., 2008). However, Brown et al.'s study found that the clinical characteristic data performed better than the fMRI measurements in the diagnosis of ADHD with an accuracy of 62.52% using data in the ADHD-200 consortium (Brown et al., 2012). Sun et al. found that some radiomic features, which described the local distribution of white matter and grey matter on structural MRI images, can classify patients with ADHD and TDCs as well as ADHD-C patients and ADHD-I patients (accuracy: 73.7% and 80.1%) (Sun et al., 2018). The present study utilized data from two centres with the largest sample size in the ADHD-200 consortium to build LASSO-SVM models based on multiple features to improve the diagnosis of ADHD. We found that radiomic features that were extracted from structural MRI images could distinguish patients with ADHD from TDCs and discern two subtypes (accuracy: 76.25% and 83.78%) with balanced sensitivity (82.85% and 84.21%) and specificity (71.11% and 83.33%) in the testing set. Furthermore, the combination of radiomic features, surface values, grey matter volume, and clinical characteristics can improve the accuracy of classifying TDCs and ADHD patients to 82.50%. Our results demonstrate that the method proposed in our study can unearth more structural MRI information that correlates with the diagnosis and subtyping of ADHD.

We utilized a novel statistical descriptor of structural MRI images, radiomics, for the diagnosis and subtyping of ADHD, achieving good performance based on multi-institutional data. Radiomics can characterize the spatial relationship of voxel intensity and was found to be a useful quantitative tool for the diagnosis of brain diseases, such as Alzheimer's disease, mild cognitive impairment, and ADHD (Yupeng Li et al., 2019; Y. Li et al., 2018; Sun et al., 2018). In our study, the radiomic features extracted from structural MRI images can diagnose ADHD and separate the two subtypes with accuracies of 76.25% and 83.78%, respectively, outperforming clinical factors, volumetric measurements, and surface values. It should be noted that integrating other categories of features with radiomic features did not improve the performance in discerning the two subtypes. The selected discriminative radiomic features for ADHD diagnosis and subtyping were principally distributed in the bilateral temporal lobe, left olfactory lobe, insula, right supplementary motor area, left occipital lobe, right frontal lobe, left hippocampus, bilateral amygdala, right calcarine, right lingual lobe, left caudate, vermis, left paracentral lobule, left supramarginal gyrus, and bilateral cerebellum (supplementary Tables S4 and S6). Previous studies also observed smaller volumes of the amygdala, caudate, hippocampus, and vermis in patients with ADHD than in TDCs (Hoogman et al., 2017; Ivanov, Murrough, Bansal, Hao, & Peterson, 2014). Differences in grey matter volume and cortical characterizations of frontal, temporal lobe, prefrontal, parietal, and occipital areas between TDCs and ADHD patients were also previously reported (Almeida et al., 2010; K. L. Narr et al., 2009; Norman et al., 2016; Philip Shaw et al., 2012; Silk et al., 2016; Tomohiro et al., 2011; Valera et al., 2007). The

cerebellum in our study contributed to both ADHD diagnosis and subtyping, and previous studies have also found cerebellar abnormalities in ADHD (Castellanos et al., 2002; Stoodley, 2016). The potential neurodevelopmental mechanisms underlying the association between radiomics of multiple brain areas and ADHD should be further investigated.

The surface values analysed in this study can quantify the morphology and complexity of the cortex and characterize cortical folding patterns, which may reflect the pathology of ADHD (Giedd & Rapoport, 2010; X. Li et al., 2007). ADHD was associated with decreased cortical thickness and delayed cortical maturation in previous studies (Narr, Woods, Lin, Kim, & Levitt, 2009; P Shaw et al., 2007). The features that described the distribution of the local cortical characterizations and white matter characterizations can discriminate between patients with ADHD and TDCs as well as between ADHD-C patients and ADHD-I patients according to Sun et al.'s study (Sun et al., 2018). The top discriminative features were alterations in cortical shape in the bilateral cuneus, left temporal lobe, and structures around the left central sulcus (Sun et al., 2018). In our study, the bilateral cuneus and subregions of the bilateral temporal lobe were also discriminative structures selected by the LASSO model, but 13 out of 18 selected surface values were distributed in the right hemisphere (supplementary Tables S4 and S6). Our results showed that surface values can distinguish ADHD from TDC with AUCs of 0.80 and 0.72 in the training and testing sets, respectively, but failed to discern two ADHD subtypes (AUC = 0.73 and 0.6 in the training and testing sets). The diagnostic performance of surface values for ADHD should be validated in future studies.

Structural MRI provides insights into GM volume and WM volume by high-resolution anatomical imaging. Brain volumetric analyses show that the GM volume of patients with ADHD was 3%−5% smaller than that of control subjects (Corina U. Greven et al., 2015). ADHD has been associated with alterations in both GM volume and WM volume in previous studies (Corina U. Greven et al., 2015; Zhao et al., 2020). However, Sun et al. reported that no volume difference was found in WM and GM between patients with ADHD and TDCs (Sun et al., 2018). Our results show that the local GM volume and local WM volume can provide limited discriminatory power between patients with ADHD and TDCs as well as between the two subtypes, with overall AUCs of 0.61–0.66.

There were several limitations in this work. First, this study only analysed the differences in the association of brain and age between TDCs and ADHD patients using a cross-sectional method and did not further investigate how ADHD affects brain development due to the limitation of data. Future work will explore longitudinal changes in the brain in ADHD patients. Second, this study did not investigate whether the psychological assessment and cognitive parameters of ADHD can improve the classification accuracy because of the absence of these data. Third, the age range of participants in this study was fairly large; the heterogeneity in brain maturation associated with age may influence the selected features and the classification performance. Finally, this study did not explore the underlying pathobiological mechanism for the correlation between structural MRI features and ADHD, which should be clarified in future studies.

Conclusions

This study established LASSO-SVM models using multiple structural MRI features, i.e., radiomic features, surface values, grey matter volumes, white matter volumes, and clinical factors, for the diagnosis and subtyping of ADHD. The radiomic feature-based models outperformed the others in discriminating patients with ADHD from TDCs as well as classifying ADHD-C patients and ADHD-I patients. Combining surface values, grey matter volume, and clinical factors with radiomics to build a hybrid model can improve the classification of TDCs and ADHD patients. The models established using quantitative features of structural MRI T1-weighted images are potential tools that are capable of informing the diagnosis and subtyping of ADHD in the clinic.

Supplementary Material

Refer to Web version on PubMed Central for supplementary material.

Acknowledgments

This study was supported by Key Technology Research and Development Program of Shandong (2017GSF218075) and Academic promotion programme of Shandong First Medical University (2019QL009).

Data analysed in our study were collected under the supports of NIMH (R01MH083246), Autism Speaks, the Stavros Niarchos Foundation, the Leon Levy Foundation, an endowment provided by Phyllis Green and Randolph Cōwen, the Commonwealth Sciences Foundation, Ministry of Health, China (200802073), the National Foundation, Ministry of Science and Technology, China (2007BAI17B03), the National Natural Sciences Foundation, China (30970802), the Funds for International Cooperation of the National Natural Science Foundation of China (81020108022), the National Natural Science Foundation of China (8100059), and Open Research Fund of the State Key Laboratory of Cognitive Neuroscience and Learning.

Data Availability Statement

Data were provided by the ADHD-200 Consortium in the international neuroimaging data-sharing initiative datasets (http://fcon_1000.projects.nitrc.org/indi/adhd200/index.html).

List of Abbreviations

AAL	automated anatomical labelling
ADHD	attention-deficit/hyperactivity disorder
ADHD-C	ADHD combined type
ADHD-H/I	ADHD hyperactive/impulsive type
ADHD-I	ADHD inattentive type
ANOVA	one-way analysis of variance
AUC	area under curve
CI	confidence interval
CPRS-LV	Conners' Parent Rating Scale-Revised-Long version

DK	Desikan-Killiany
fMRI	functional magnetic resonance imaging
FOV	field of view
GLCM	grey-level co-occurrence matrix
GLRLM	grey-level run length matrix
GM	grey matter
IQ	intelligence quotient
KSADS-PL	Schedule of Affective Disorders and Schizophrenia for Children-Present and Lifetime Version
LASSO	least absolute shrinkage and selection operator
MRI	magnetic resonance imaging
NIDM	neighbourhood intensity difference matrix
NIMH	National Institute of Mental Health
NYU	New York University
PU	Peking University
rho	Spearman's correlation coefficient
ROC	receiver operating characteristic
ROI	region-of-interest
SVM	support vector machine
TDC	typically developing controls
TE	echo time
TR	repetition time
VBM	voxel-based method
WM	white matter

References

Aerts HJ, Velazquez ER, Leijenaar RT, Parmar C, Grossmann P, Carvalho S, … Lambin P (2014). Decoding tumour phenotype by noninvasive imaging using a quantitative radiomics approach. Nat Commun, 5, 4006. doi:10.1038/ncomms5006 [PubMed: 24892406]

Al-Radaideh A, Athamneh I, Alabadi H, & Hbahbih M (2019). Cortical and Subcortical Morphometric and Iron Changes in Relapsing-Remitting Multiple Sclerosis and Their Association with White Matter T2 Lesion Load : A 3-Tesla Magnetic Resonance Imaging Study. Clin Neuroradiol, 29(1), 51–64. doi:10.1007/s00062-017-0654-0 [PubMed: 29299614]

Almeida LG, Ricardo-Garcell J, Prado H, Barajas L, Fernández-Bouzas A, Avila D, & Martínez RB (2010). Reduced right frontal cortical thickness in children, adolescents and adults with ADHD and its correlation to clinical variables: a cross-sectional study. J Psychiatr Res, 44(16), 1214–1223. doi:10.1016/j.jpsychires.2010.04.026 [PubMed: 20510424]

Berger A, & Posner MI (2000). Pathologies of brain attentional networks. Neuroscience & Biobehavioral Reviews, 24(1), 3–5. [PubMed: 10654653]

Brinson H (2014). Imaging the ADHD brain: disorder-specificity, medication effects and clinical translation. Expert Review of Neurotherapeutics, 14(5), 519. [PubMed: 24738703]

Brown MR, Sidhu GS, Greiner R, Asgarian N, Bastani M, Silverstone PH, … Dursun SM (2012). ADHD-200 Global Competition: diagnosing ADHD using personal characteristic data can outperform resting state fMRI measurements. Front Syst Neurosci, 6, 69. doi:10.3389/fnsys.2012.00069 [PubMed: 23060754]

Castellanos FX, Lee PP, Sharp W, Jeffries NO, Greenstein DK, Clasen LS, … Rapoport JL (2002). Developmental trajectories of brain volume abnormalities in children and adolescents with attention-deficit/hyperactivity disorder. Jama, 288(14), 1740–1748. doi:10.1001/jama.288.14.1740 [PubMed: 12365958]

Chi-Hua C, Mark F, Gutiérrez ED, Panizzon MS, Eyler LT, Eero V, … Jernigan TL (2013). Genetic topography of brain morphology. Proceedings of the National Academy of Sciences of the United States of America, 110(42), 17089–17094. [PubMed: 24082094]

Corbit JD, & Garbary DJ (1995). Fractal Dimension as a Quantitative Measure of Complexity in Plant Development. Royal Society Proceedings B Biological Sciences, 262(1363), 1–6.

Dahnke R, Yotter RA, & Gaser C (2013). Cortical thickness and central surface estimation. NeuroImage, 65, 336–348. doi:10.1016/j.neuroimage.2012.09.050 [PubMed: 23041529]

Draper A, Jackson GM, Morgan PS, & Jackson SR (2016). Premonitory urges are associated with decreased grey matter thickness within the insula and sensorimotor cortex in young people with Tourette syndrome. J Neuropsychol, 10(1), 143–153. doi:10.1111/jnp.12089 [PubMed: 26538289]

Friedman J, Hastie T, & Tibshirani R (2010). Regularization Paths for Generalized Linear Models via Coordinate Descent. J Stat Softw, 33(1), 1–22. [PubMed: 20808728]

Frodl T, & Skokauskas N (2012). Meta-analysis of structural MRI studies in children and adults with attention deficit hyperactivity disorder indicates treatment effects. Acta Psychiatrica Scandinavica, 125(2), 114–126. [PubMed: 22118249]

Gaser, & Dahnke R (2016). CAT - A Computational Anatomy Toolbox for the Analysis of Structural MRI Data.

Giedd JN, & Rapoport JL (2010). Structural MRI of pediatric brain development: what have we learned and where are we going? Neuron, 67(5), 728–734. doi:10.1016/j.neuron.2010.08.040 [PubMed: 20826305]

Greven CU, Bralten J, Mennes M, O'Dwyer L, van Hulzen KJ, Rommelse N, … Heslenfeld D (2015). Developmentally stable whole-brain volume reductions and developmentally sensitive caudate and putamen volume alterations in those with attention-deficit/hyperactivity disorder and their unaffected siblings. Jama Psychiatry, 72(5), 490. [PubMed: 25785435]

Greven CU, Bralten J, Mennes M, O'Dwyer L, van Hulzen KJE, Rommelse N, … Heslenfeld D (2015). Developmentally Stable Whole-Brain Volume Reductions and Developmentally Sensitive Caudate and Putamen Volume Alterations in Those With Attention-Deficit/Hyperactivity Disorder and Their Unaffected Siblings. JAMA Psychiatry, 72(5), 490–499. [PubMed: 25785435]

Guo X, An X, Kuang D, Zhao Y, & He L (2014, 2014//). ADHD-200 Classification Based on Social Network Method. Paper presented at the Intelligent Computing in Bioinformatics, Cham.

Gutman B, Wang Y, Morra J, Toga AW, & Thompson PM (2009). Disease classification with hippocampal shape invariants. Hippocampus, 19(6), 572–578. doi:10.1002/hipo.20627 [PubMed: 19437498]

HD-200 C (2012). The ADHD-200 Consortium: A Model to Advance the Translational Potential of Neuroimaging in Clinical Neuroscience. Frontiers in systems neuroscience, 6, 62–62. doi:10.3389/fnsys.2012.00062 [PubMed: 22973200]

Hoogman M, Bralten J, Hibar DP, Mennes M, Zwiers MP, Schweren LSJ, … Jahanshad N (2017). Subcortical brain volume differences in participants with attention deficit hyperactivity disorder in

children and adults: a cross-sectional mega-analysis. Lancet Psychiatry, 4(4), 310–319. [PubMed: 28219628]

Ivanov I, Murrough JW, Bansal R, Hao X, & Peterson BS (2014). Cerebellar morphology and the effects of stimulant medications in youths with attention deficit-hyperactivity disorder. Neuropsychopharmacology, 39(3), 718–726. doi:10.1038/npp.2013.257 [PubMed: 24077064]

Li X, Jiang J, Zhu W, Yu C, Sui M, Wang Y, & Jiang T (2007). Asymmetry of prefrontal cortical convolution complexity in males with attention-deficit/hyperactivity disorder using fractal information dimension. Brain and Development, 29(10), 649–655. doi:10.1016/j.braindev.2007.04.008 [PubMed: 17573219]

Li Y, Jiang J, Lu J, Jiang J, Zhang H, & Zuo C (2019). Radiomics: a novel feature extraction method for brain neuron degeneration disease using (18)F-FDG PET imaging and its implementation for Alzheimer's disease and mild cognitive impairment. Therapeutic advances in neurological disorders, 12, 1756286419838682–1756286419838682. doi:10.1177/1756286419838682 [PubMed: 30956687]

Li Y, Jiang J, Shen T, Wu P, & Zuo C (2018, 18–21 July 2018). Radiomics features as predictors to distinguish fast and slow progression of Mild Cognitive Impairment to Alzheimer's disease. Paper presented at the 2018 40th Annual International Conference of the IEEE Engineering in Medicine and Biology Society (EMBC).

Lohmann P, Meißner A-K, Kocher M, Bauer EK, Werner J-M, Fink GR, … Galldiks N (2021). Feature-based PET/MRI radiomics in patients with brain tumors. Neuro-Oncology Advances, 2(Supplement_4), iv15–iv21. doi:10.1093/noajnl/vdaa118 [PubMed: 33521637]

Lu L, Zhang L, Tang S, Bu X, Chen Y, Hu X, … Huang X (2019). Characterization of cortical and subcortical abnormalities in drug-naive boys with attention-deficit/hyperactivity disorder. Journal of affective disorders, 250, 397–403. doi:10.1016/j.jad.2019.03.048 [PubMed: 30877863]

Luders E, Thompson PM, Narr KL, Toga AW, Jancke L, & Gaser C (2006). A curvature-based approach to estimate local gyrification on the cortical surface. NeuroImage, 29(4), 1224–1230. doi:10.1016/j.neuroimage.2005.08.049 [PubMed: 16223589]

Madeira N, Duarte J, Martins R, Costa G, Macedo A, & Castelo-Branco M (2020). Morphometry and gyrification in bipolar disorder and schizophrenia: A comparative MRI study. NeuroImage Clinical, 26, 102220. doi:10.1016/j.nicl.2020.102220 [PubMed: 32146321]

Narr KL, Woods RP, Lin J, Kim J, & Levitt JG (2009). Widespread Cortical Thinning Is a Robust Anatomical Marker for Attention-Deficit/Hyperactivity Disorder. Journal of the American Academy of Child & Adolescent Psychiatry, 48(10), 1014–1022. [PubMed: 19730275]

Narr KL, Woods RP, Lin J, Kim J, Phillips OR, Del'Homme M, … Levitt JG (2009). Widespread cortical thinning is a robust anatomical marker for attention-deficit/hyperactivity disorder. J Am Acad Child Adolesc Psychiatry, 48(10), 1014–1022. doi:10.1097/CHI.0b013e3181b395c0 [PubMed: 19730275]

Nguyen AV, Blears EE, Ross E, Lall RR, & Ortega-Barnett J (2018). Machine learning applications for the differentiation of primary central nervous system lymphoma from glioblastoma on imaging: a systematic review and meta-analysis. Neurosurgical Focus FOC, 45(5), E5. doi:10.3171/2018.8.focus18325

NIMH. National Institue of Mental Health: Attention-Deficit/Hyperactivity Disorder. Retrieved from https://www.nimh.nih.gov/health/topics/attention-deficit-hyperactivity-disorder-adhd/index.shtml

Norman LJ, Carlisi C, Lukito S, Hart H, Mataix-Cols D, Radua J, & Rubia K (2016). Structural and Functional Brain Abnormalities in Attention-Deficit/Hyperactivity Disorder and Obsessive-Compulsive Disorder: A Comparative Meta-analysis. JAMA Psychiatry, 73(8), 815–825. doi:10.1001/jamapsychiatry.2016.0700 [PubMed: 27276220]

Overmeyer S,., Bullmore ET, Suckling J,., Simmons A,., Williams SC, Santosh PJ, & Taylor E,. (2001). Distributed grey and white matter deficits in hyperkinetic disorder: MRI evidence for anatomical abnormality in an attentional network. Psychological Medicine, 31(8), 1425–1435. [PubMed: 11722157]

Park JE, Kim HS, Jo Y, Yoo R-E, Choi SH, Nam SJ, & Kim JH (2020). Radiomics prognostication model in glioblastoma using diffusion- and perfusion-weighted MRI. Scientific Reports, 10(1), 4250. doi:10.1038/s41598-020-61178-w [PubMed: 32144360]

Polanczyk G, & Rohde LA (2007). Epidemiology of attention-deficit/hyperactivity disorder across the lifespan. Current Opinion in Psychiatry, 20(4), 386. [PubMed: 17551354]

Port JD (2018). Diagnosis of Attention Deficit Hyperactivity Disorder by Using MR Imaging and Radiomics: A Potential Tool for Clinicians. Radiology, 287(2), 631–632. doi:10.1148/radiol.2018172804 [PubMed: 29668406]

Rish I, Thyreau B, Thirion B, Plaze M, Pailleremartinot M, Martelli C, … Cecchi GA (2009). Discriminative Network Models of Schizophrenia. 22, 252–260.

Sato JR, Hoexter MQ, Fujita A, & Rohde LA (2012). Evaluation of pattern recognition and feature extraction methods in ADHD prediction. Journal of Business Economics & Management, 13(4), 688–704.

Shaw P, Eckstrand K, Sharp W, Blumenthal J, Lerch JP, Greenstein D, … Rapoport JL (2007). Attention-deficit/hyperactivity disorder is characterized by a delay in cortical maturation. Proceedings of the National Academy of Sciences of the United States of America, 104(49), 19649–19654. [PubMed: 18024590]

Shaw P, Malek M, Watson B, Sharp W, Evans A, & Greenstein D (2012). Development of Cortical Surface Area and Gyrification in Attention-Deficit/Hyperactivity Disorder. Biological Psychiatry, 72(3), 191–197. [PubMed: 22418014]

Shen H, Wang L, Liu Y, & Hu D (2010). Discriminative analysis of resting-state functional connectivity patterns of schizophrenia using low dimensional embedding of fMRI. NeuroImage, 49(4), 3110–3121. [PubMed: 19931396]

Silk TJ, Beare R, Malpas C, Adamson C, Vilgis V, Vance A, & Bellgrove MA (2016). Cortical morphometry in attention deficit/hyperactivity disorder: Contribution of thickness and surface area to volume. Cortex, 82, 1–10. doi:10.1016/j.cortex.2016.05.012 [PubMed: 27268101]

Sordo M, & Zeng Q (2005). On Sample Size and Classification Accuracy: A Performance Comparison, Berlin, Heidelberg.

Stoodley CJ (2016). The Cerebellum and Neurodevelopmental Disorders. Cerebellum (London, England), 15(1), 34–37. doi:10.1007/s12311-015-0715-3

Sun H, Chen Y, Huang Q, Lui S, Huang X, Shi Y, … Gong Q (2018). Psychoradiologic Utility of MR Imaging for Diagnosis of Attention Deficit Hyperactivity Disorder: A Radiomics Analysis. Radiology, 287(2), 620–630. doi:10.1148/radiol.2017170226 [PubMed: 29165048]

Tang X, Seymour K, Crocetti D, Miller M, Mostofsky S, & Rosch K (2019). Response control correlates of anomalous basal ganglia morphology in boys, but not girls, with attention-deficit/hyperactivity disorder. Behavioural brain research, 367, 117–127. doi:10.1016/j.bbr.2019.03.036 [PubMed: 30914308]

Tibshirani R (2011). Regression shrinkage and selection via the lasso: a retrospective. Journal of the Royal Statistical Society: Series B (Statistical Methodology), 73(3), 273–282. doi:10.1111/j.1467-9868.2011.00771.x

Tomohiro N, Joaquim R, Katya R, & David MC (2011). Gray matter volume abnormalities in ADHD: voxel-based meta-analysis exploring the effects of age and stimulant medication. American Journal of Psychiatry, 168(11), 1154–1163.

Ulke C, Rullmann M, Huang J, Luthardt J, Becker G, Patt M, … Strauß M (2019). Adult attention-deficit/hyperactivity disorder is associated with reduced norepinephrine transporter availability in right attention networks: a (S,S)-O-[C]methylreboxetine positron emission tomography study. Translational psychiatry, 9(1), 301. doi:10.1038/s41398-019-0619-y [PubMed: 31732713]

Valera EM, Faraone SV, Murray KE, & Seidman LJ (2007). Meta-analysis of structural imaging findings in attention-deficit/hyperactivity disorder. Biological Psychiatry, 61(12), 1361–1369. [PubMed: 16950217]

Vilgis V, Sun L, Chen J, Silk TJ, & Vance A (2016). Global and local grey matter reductions in boys with ADHD combined type and ADHD inattentive type. Psychiatry Research Neuroimaging, 254, 119–126. [PubMed: 27399309]

Visser SN, Danielson ML, Bitsko RH, Holbrook JR, Kogan MD, Ghandour RM, … Blumberg SJ (2014). Trends in the parent-report of health care provider-diagnosed and medicated attention-deficit/hyperactivity disorder: United States, 2003–2011. J Am Acad Child Adolesc Psychiatry, 53(1), 34–46.e32. [PubMed: 24342384]

Wang Y, Sun K, Liu Z, Chen G, Jia Y, Zhong S, … Tian J (2020). Classification of Unmedicated Bipolar Disorder Using Whole-Brain Functional Activity and Connectivity: A Radiomics Analysis. Cereb Cortex, 30(3), 1117–1128. doi:10.1093/cercor/bhz152 [PubMed: 31408101]

Wolf R, Hildebrandt V, Schmitgen M, Pycha R, Kirchler E, Macina C, … Huber M (2020). Aberrant Gray Matter Volume and Cortical Surface in Paranoid-Type Delusional Disorder. Neuropsychobiology, 1–10. doi:10.1159/000505601 [PubMed: 32454501]

Wu Y, Jiang J-H, Chen L, Lu J-Y, Ge J-J, Liu F-T, … Wang J (2019). Use of radiomic features and support vector machine to distinguish Parkinson's disease cases from normal controls. Annals of Translational Medicine, 7(23), 773. [PubMed: 32042789]

Yan CG, Wang XD, Zuo XN, & Zang YF (2016). DPABI: Data Processing & Analysis for (Resting-State) Brain Imaging. Neuroinformatics, 14(3), 339–351. doi:10.1007/s12021-016-9299-4 [PubMed: 27075850]

Yotter RA, Nenadic I, Ziegler G, Thompson P, & Gaser C (2011b). Local cortical surface complexity maps from spherical harmonic reconstructions. NeuroImage, 56(3), 961–973. doi:10.1016/j.neuroimage.2011.02.007 [PubMed: 21315159]

Yotter RA, Nenadic I, Ziegler G, Thompson PM, & Gaser C (2011). Local cortical surface complexity maps from spherical harmonic reconstructions. NeuroImage, 56(3), 961–973. doi:10.1016/j.neuroimage.2011.02.007 [PubMed: 21315159]

Zhang L, Fried DV, Fave XJ, Hunter LA, Yang J, & Court LE (2015). IBEX: an open infrastructure software platform to facilitate collaborative work in radiomics. Med Phys, 42(3), 1341–1353. doi:10.1118/1.4908210 [PubMed: 25735289]

Zhao Y, Cui D, Lu W, Li H, Zhang H, & Qiu J (2020). Aberrant gray matter volumes and functional connectivity in adolescent patients with ADHD. Journal of magnetic resonance imaging : JMRI, 51(3), 719–726. doi:10.1002/jmri.26854 [PubMed: 31265198]

Zheng F, Liu Y, Yuan Z, Gao X, He Y, Liu X, … Qiu J (2019). Age-related changes in cortical and subcortical structures of healthy adult brains: A surface-based morphometry study. J Magn Reson Imaging, 49(1), 152–163. doi:10.1002/jmri.26037 [PubMed: 29676856]

Zhu CZ, Zang YF, Cao QJ, Yan CG, He Y, Jiang TZ, … Wang YF (2008). Fisher discriminative analysis of resting-state brain function for attention-deficit/hyperactivity disorder. NeuroImage, 40(1), 110–120. doi:10.1016/j.neuroimage.2007.11.029 [PubMed: 18191584]

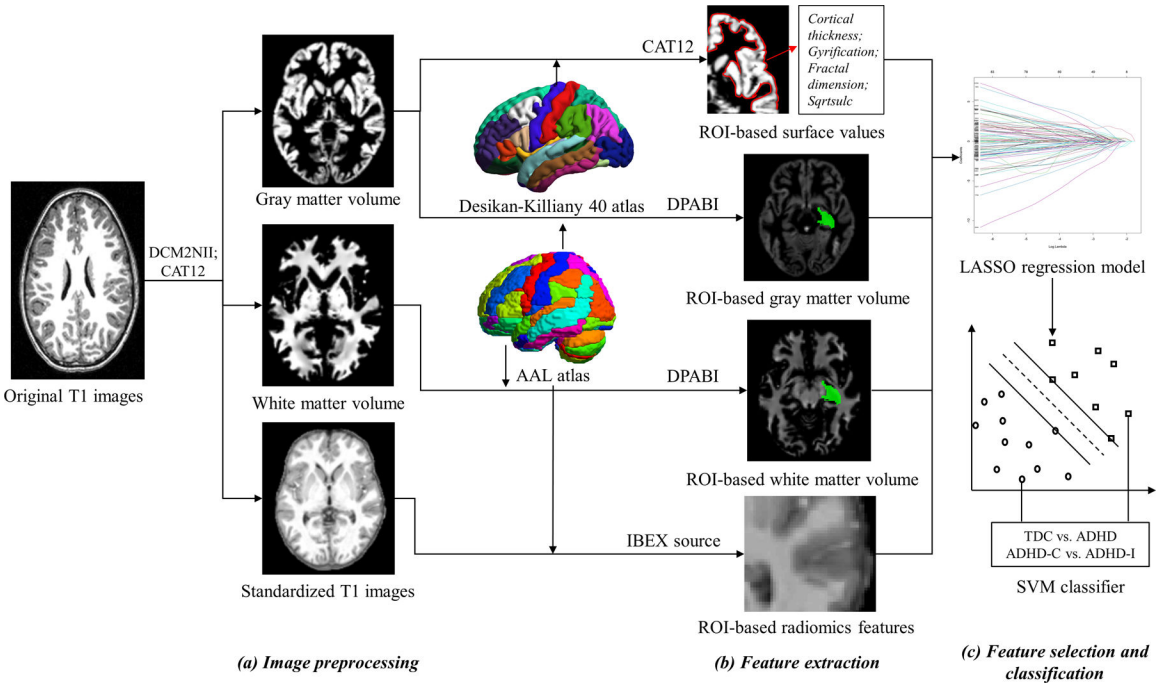

Figure 1.

The workflow of image processing (a), feature extraction (b), and feature selection and classification (c) performed in this study. The software and templates used in each step are also shown. LASSO: least absolute shrinkage and selection operator; SVM: support vector machine.

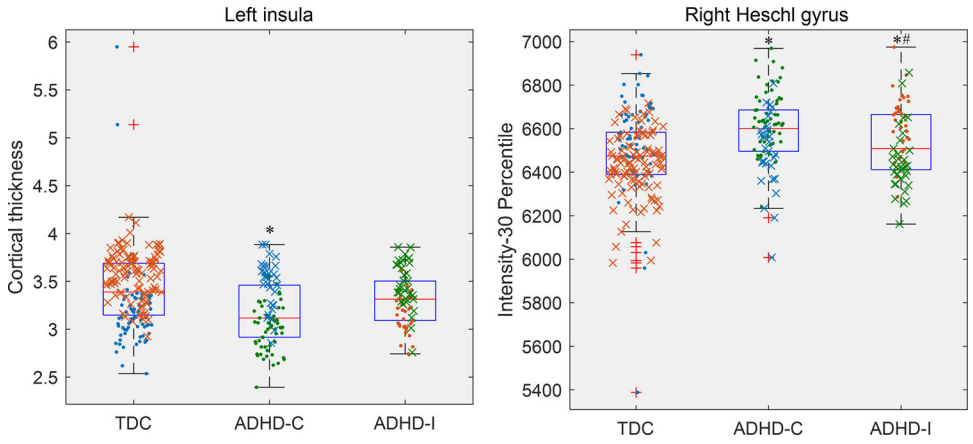

Figure 2.

Boxplots and data distribution of two representative discriminative features: cortical thickness of the left insula (a surface value) (a) and intensity-30 percentile of the right Heschl gyrus (a radiomic feature) (b). The horizontal line inside the box represents the median. The upper and lower whiskers extend to the highest and lowest values within the 1.5*IQR of the 0.75 quartile and 0.25 quartile, respectively. Outliers are plotted as plus signs. '·' represents data from New York University (NYU); 'x' represents data from Peking University (PU); '*' Compared to the typically developing controls (TDC), $P < 0.05$; '#' Compared to the ADHD combined type (ADHD-C), $P < 0.05$.

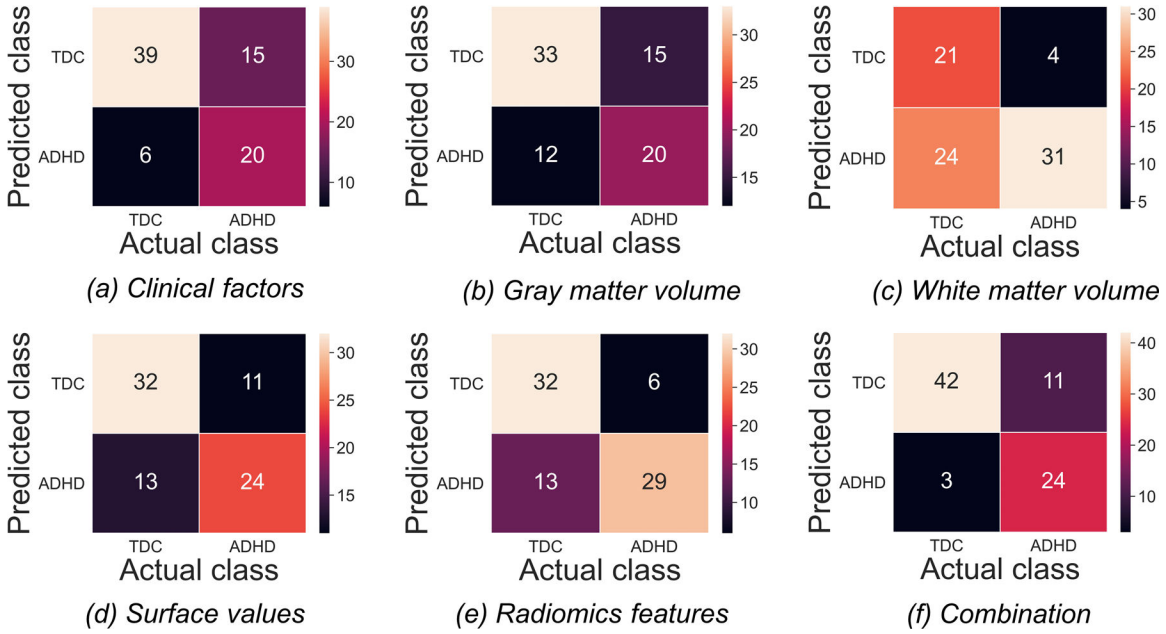

Figure 3.

The confusion matrices for the classification of patients with attention-deficit/hyperactivity disorder (ADHD) and typically developing controls (TDCs) based on different categories of features in the testing set. Each column/row of a confusion matrix represents the number of patients in an actual/predicted class.

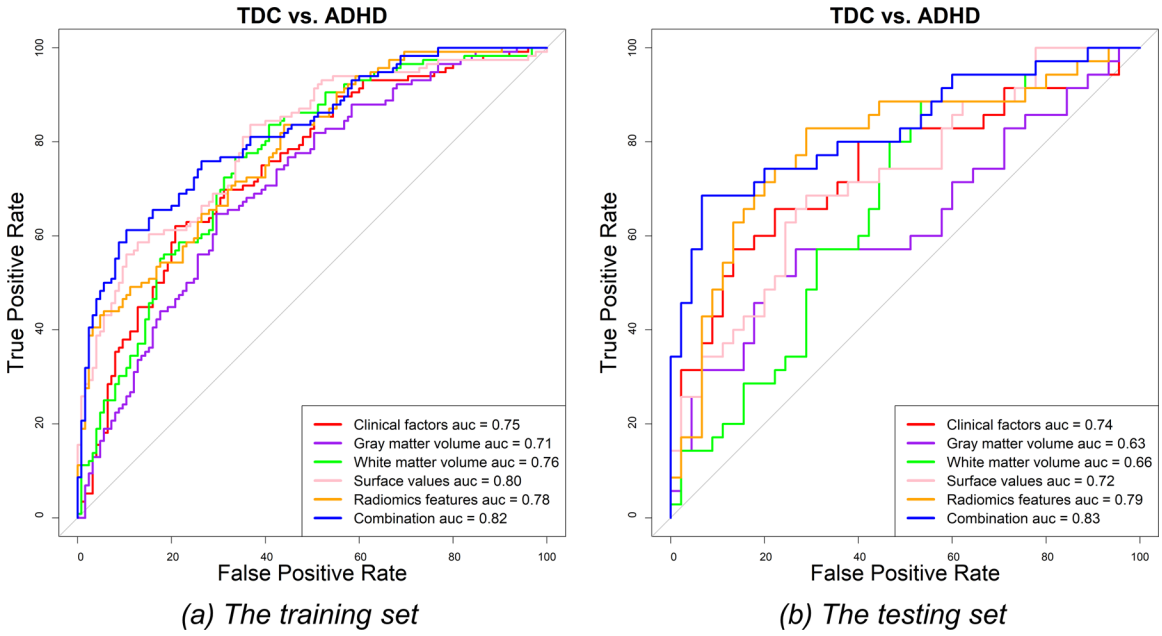

Figure 4.

The ROC curves for the discrimination between patients with attention-deficit/hyperactivity disorder (ADHD) and typically developing controls (TDCs) in the training (a) and testing (b) sets.

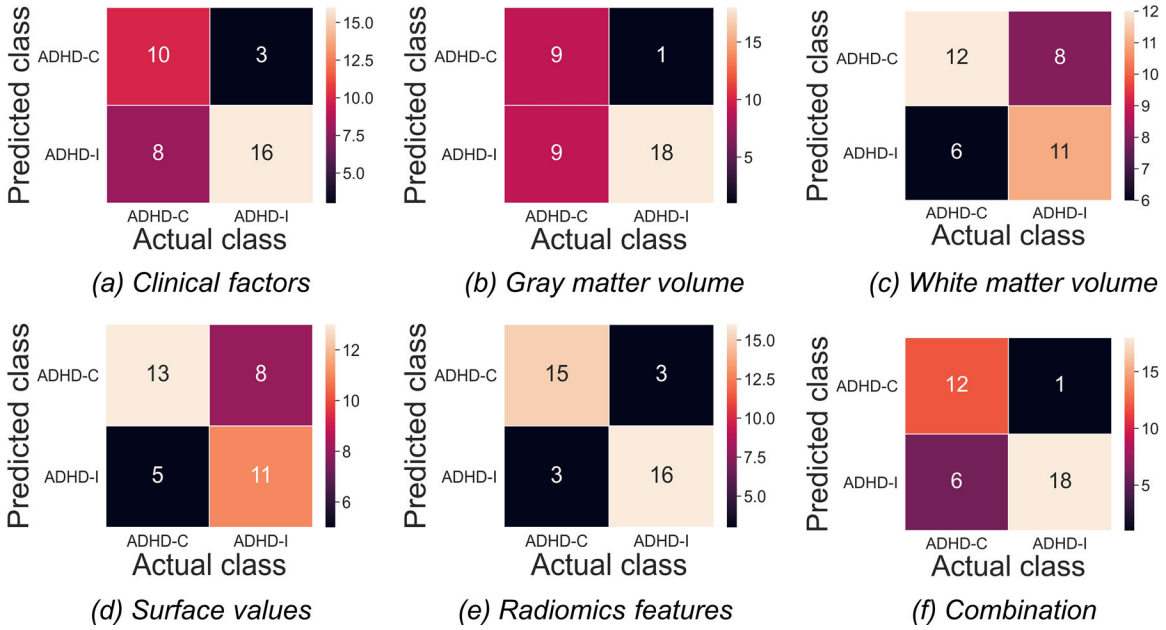

Figure 5.

The confusion matrices for the classification of attention-deficit/hyperactivity disorder (ADHD) inattentive type (ADHD-I) patients and ADHD combined type (ADHD-C) patients based on different categories of features in the testing set. Each column/row of a confusion matrix represents the number of patients in an actual/predicted class.

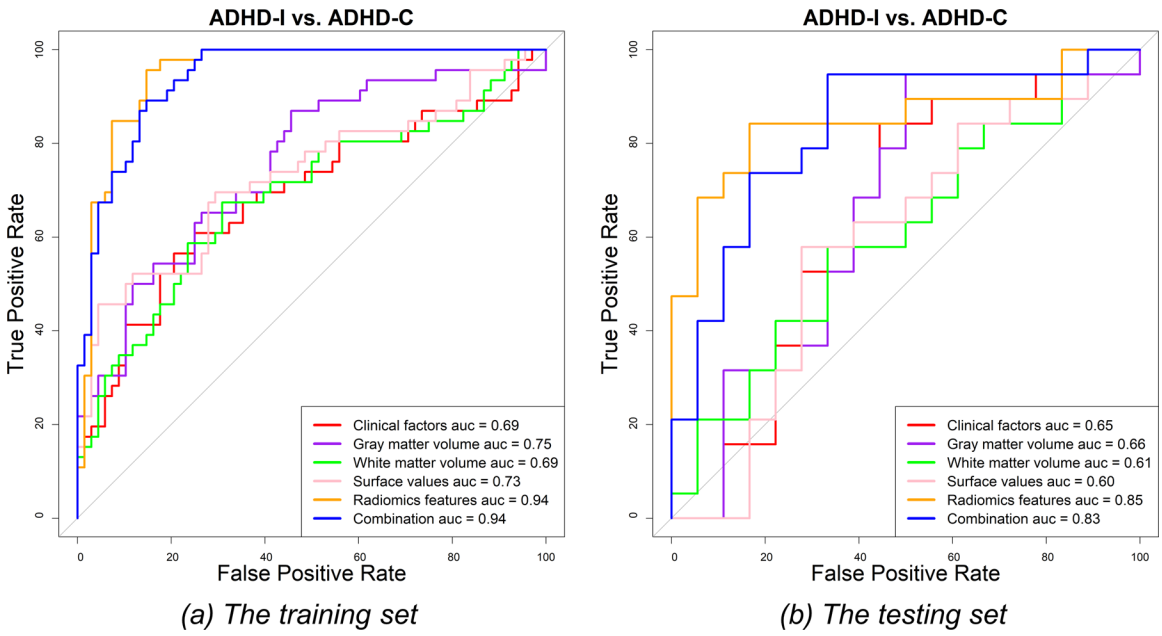

Figure 6.

The ROC curves for the discrimination between attention-deficit/hyperactivity disorder (ADHD) inattentive type (ADHD-I) patients and ADHD combined type (ADHD-C) patients in the training (a) and testing (b) sets.

Table 1.

The demographic information of all participants from two medical centers.

Clinical factors	NYU (n = 155)			PU (n = 166)			P values among three groups	P values in multiple comparison test		
	TDC (n = 67)	ADHD-C (n = 56)	ADHD-I (n = 32)	TDC (n = 103)	ADHD-C (n = 30)	ADHD-I (n = 33)		TDC vs. ADHD-C	TDC vs. ADHD-I	ADHD-C vs. ADHD-I
Gender (M/F)	30/37	45/11	22/10	62/41	30/0	27/6	$2.11*10^{-7}$	$3.08*10^{-7}$	$5.00*10^{-3}$	P > 0.05
Age (years) (mean ± SD)	12.1±2.9	11.0±2.5	12.3±2.6	11.4±1.9	11.8±1.8	12.3±2.1	0.04	P > 0.05	P > 0.05	0.03
Verbal IQ (mean ± SD)	112.1±13.9	108.8±13.2	107.9±17.1	120.2±14.1	115.9±17.1	106.6±14.7	$1.56*10^{-5}$	$9.60*10^{-3}$	$2.02*10^{-5}$	P > 0.05
Performance IQ (mean ± SD)	106.9±14.2	102.9±12.1	106.8±15.0	111.5±14.6	98.5±12.1	97.7±10.5	$4.64*10^{-6}$	$2.80*10^{-5}$	$7.24*10^{-4}$	P > 0.05

ADHD: attention-deficit/hyperactivity disorder; ADHD-C: ADHD combined type; ADHD-I: ADHD inattentive type; NYU: New York University; PU: Peking University; SD: standard deviation; TDC: typically developing controls.